Assessment of Similitude Behavior in Natural Frequencies of Printed Turbine Blade

MUHAMMAD Usman Safdar[1], *SHEN Xing*[2*], *EIMAN B. Saheby*[1]

1. State Key Lab of Mechanics and Control for Aerospace Structures, College of Aeronautics, Nanjing University of Aeronautics and Astronautics, Nanjing 210016, P. R. China;

2. Graduate School , Chinese Aeronautical Establishment, Yangzhou 225111, P. R. China

(Received 5 May 2024; revised 22 June 2024; accepted 23 July 2024)

Abstract: Improving structures involves comparing old and new designs on a key parameter. Calculating the percent change in performance is a method to assess. This paper proposes a cost-effective analogy by generating replicas of additive manufactured aluminum alloy (AlSi10Mg) body-centered cubic lattice (BCC) based turbine blade (T106C) with the same in poly-lactic acid (PLA) material and their comparison in the context of percent change for natural frequencies. Initially, a cavity is created inside the turbine blade (hollow blade). Natural frequencies are obtained experimentally and numerically by incorporating BCC at 50% and 80% of the cavity length into the hollow blade for both materials. The cost of manufacturing the metal blades is 90% more than that of the PLA blades. The two material blade designs show a similar percentage variation, as the first-order mode enhancs more than 5% and the second-order mode more than 4%. To observe the behavior in another material, both blades are analyzed numerically with a nickel-based U-500 material, and the same result is achieved, describing that percent change between designs can be verified using the PLA material.

Key words: AlSi10Mg; poly-lactic acid(PLA); U-500; T106C blade; BCC lattice structure

CLC number: V232.4 **Document code:** A **Article ID:** 1005-1120(2024)04-0488-14

0 Introduction

With time, the advancement in additive manufacturing is underway with different and complex structures being additive manufactured. One of the interesting complex designs is the lattice structure. According to Ref.[1], a lattice structure is a truss-like structure formed by unit cells arranged in a regular pattern. Different types of lattice structures of unit cells can be seen in Fig. 1[2]. These recurrent unit cells are arranged in all directions to create a whole structure, serving as building blocks. In the past few years, much work has been done on their utilization inside different structures to enhance their strength and mechanical performance. Kulangara et al.[3] utilized a honeycomb lattice structure on a spur gear by considering weight reduction as the primary objective. The stress and displacements of the modified spur gear were compared with the full part and concluded the same stress levels at 19% volume reduction. Yin et al.[4] introduced a double curvature composite sandwich hood with a pyramidal lattice core as an alternative to the automobile engine hood for better pedestrian safety performance compared to their baseline hood design which was without a lattice core and reduced the weight by 25% (Fig.2 (a)). Magerramova et al.[5] integrated cellular lattice structure inside the fan blades of a gas turbine engine (GTE) and investigated that the strength-to-mass ratio was 1.76—2.36 times greater than that of the solid. The weight reduced by 27%—64% less than all metal blades, and stress was found to be 2 times less (Fig. 2(b)). Du et al.[6] developed a

*Corresponding author, E-mail address: shenx@nuaa.edu.cn.

How to cite this article: MUHAMMAD Usman Safdar, SHEN Xing, EIMAN B. Saheby. Assessment of similitude behavior in natural frequencies of printed turbine blade[J]. Transactions of Nanjing University of Aeronautics and Astronautics, 2024, 41(4):488-501.

http://dx.doi.org/10.16356/j.1005-1120.2024.04.006

novel lattice structure, inspired by a beetle front wing. Their goal was to investigate the effects of processing parameters on densification behavior, microstructure, and mechanical properties. The additive manufacturing used in manufacturing complex structures is expensive. Effective methods are needed to ensure accuracy based on operating conditions.

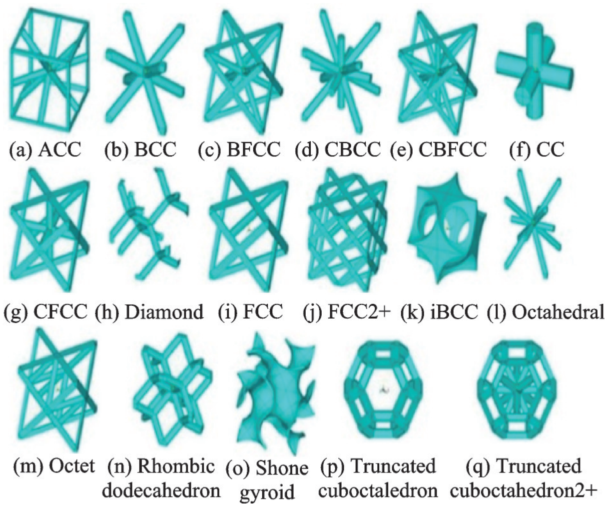

Fig.1 Examples of lattice structure unit cells[2]

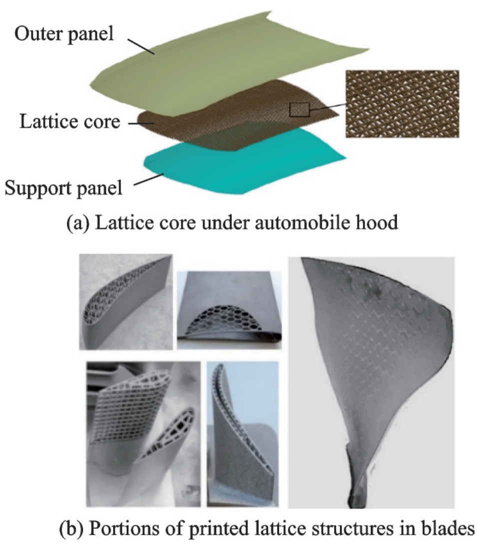

Fig.2 Lattice-based products

Researching and developing various stages of turbojet engines can incur significant costs, particularly when testing prototypes for validation. From Ref. [7], it is known that a low-pressure turbine (LPT) is 30% of the total engine weight, and reducing its mass can increase the overall performance (life, operational cost, operational speed, etc.). The mass reduction of the turbine blades can be achieved by changing materials[8-10] and decreasing the number of blades with the usage of high-lifting airfoils[11-13]. Antorkas et al.[14] worked on the topology optimization for volume reduction of a T106C LPT blade, based on static structural analysis. The blade mass was reduced by 50%, with two internal cavities covering 90% of the span. However, topology optimization gave a huge advancement in decreasing the mass but failed to address the vibrational behavior of the blade in their study. Since turbine blades have to go through a lot of adverse stresses and aero-elastic forces during their operational life. An improper design of the blade (aerodynamic shape, material, fatigue, flutter) can be catastrophic for the whole engine. As seen by research[15], LPT blades are found more prone to failure because of their mass, high aspect ratio lengths, and high lifting profiles, causing them to vibrate in the engine during transient loads. Hence, reduction of mass is not the only aspect, an enhancement of natural frequencies is also important.

To understand the vibrational behavior of any structure, experimental and numerical modal testing and analysis are used by the designers[16-17]. Even though theoretical and numerical techniques are valuable tools, the predicted results need to be verified by experimental testing before the concept can be utilized in production. In this manner, the intended reliability, performance, and safety can be achieved whether applied to the validation of a simple or complex system[18].

Extensive research on experimental modal analysis (EMA) and numerical modal and harmonic analysis (NMHA) from 2004—2022[19-32] have been conducted on the single blade or a whole rotor disk to find the natural frequencies for operational speed, vibrational failure prediction and structural health monitoring. However, the usage of the lattice concept for optimizing the turbine blade is reported by Hussain et al.[33-34], in which they utilized lattice structures to enhance the natural frequencies and decreased mass of a metal 3D-printed turbine blade, verifying it by EMA and NMHA. They filled the blade with an octet lattice structure and worked by analyzing different strut thicknesses (0.75, 0.5 and

0.25 mm) of the lattice structure onto the natural frequencies of the blade. They concluded that the 0.25 mm strut thickness octet truss lattice in the turbine blade shown in Fig.3 enhanced the natural frequencies better than the other strut thickness lattices.

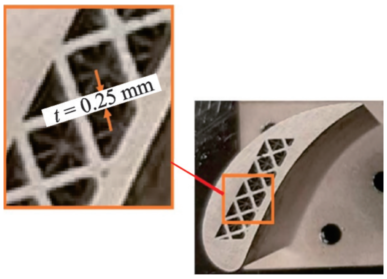

Fig.3 Metallic turbine blade with octet truss lattice of 0.25 mm strut thickness

Metal printing for the blades can be expensive. An alternate method is needed to do wider research on complex geometrical structures like lattices. Bian et al.[35] investigated the compression behaviors of BCC lattice structures additive manufactured by using poly-lactic acid (PLA), AlSi10Mg and polyamide 12 (PA12). Although the three component materials have different mechanical properties, they observed that the built lattice structures showed comparable stress-strain curve features and almost the same deformation mode. This led them to employ PLA and PA12 as constituent materials for investigating the mechanical response rather than utilizing metals to decrease the cost and ensure generic results.

Few studies have compared the mechanical response of lattice structures with different materials. None has explored the dynamic response of lattices integrated into a structure. This study aims to fill this gap by analyzing the percent change in natural frequencies between hollow and body centered cubic (BCC) structutes of lattice-based turbine blades made from AlSi10Mg and PLA plastic. To observe differences in performance, the comparison involves modal analysis. A nickel-based alloy namely Udiemt-500 (U-500) material is also numerically analyzed on a similar basis to aluminum and PLA blades for natural frequency percentages for validation. This paper will also show the impact of lattice structures on their potential to enhance the natural frequencies of the blade.

1 Methodology

1.1 Baseline blade models

T106C is a high aspect ratio, high lifting profile turbine blade. It is characterized as a high-lifting airfoil because of its high degree of camber with sharp leading, trailing edges and a maximum thickness of $0.35C_x$ (35% of chord length)[36]. The removal of mass from the blade is beneficial to the blade, as mass is inversely proportional to the square of natural frequency. For this study, a blade model with a cavity ranging from 10% to 65%[14] along the camber line to cover the entire span is created to reduce mass and increase the natural frequencies. It can be seen from Fig.4. The upper surface $V_u(x)$ and lower surface $V_l(x)$ are the curve functions of the T106C blade for a chord length (c), whereas the upper and lower curve functions of the cavity represent $C_u(x)$ and $C_l(x)$. The area (A_{T106C}) and moment of inertia (I_{T106C}) sum up all small rectangular sections ($(V_u - V_l)dx$) within the blade. By subtracting the cavity area (A_{cavity}) and its moment of inertia (I_{cavity}), the total area (A_{HB}) and total moment of inertia (I_{HB}) of the hollow blade are found. The inertia of each section is taken about the neutral surface position ($\bar{v}$) defined for the whole cross-section[37].

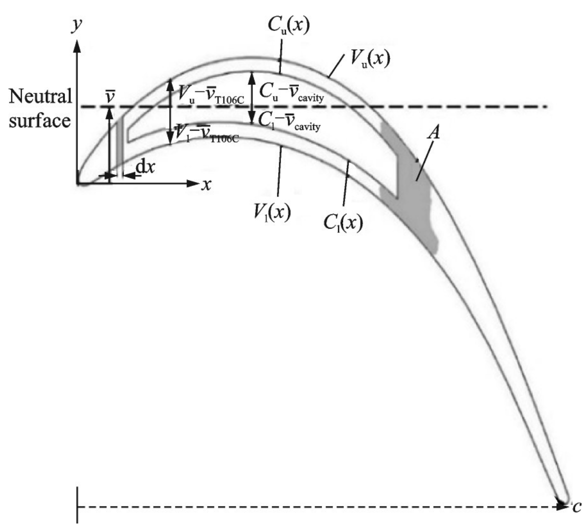

Fig.4 Quantities for determining and estimating the bending inertia of a hollow airfoil section

$$A_{\mathrm{T106C}} = \int_0^c (V_{\mathrm{u}} - V_{\mathrm{l}})\,\mathrm{d}x \tag{1}$$

$$\bar{v}_{\mathrm{T106C}} = \frac{1}{A_{\mathrm{T106C}}}\left[\int_0^c \frac{1}{2}(V_{\mathrm{u}}^2 - V_{\mathrm{l}}^2)\,\mathrm{d}x\right] \tag{2}$$

$$I_{\mathrm{T106C}} = \int_0^c \frac{1}{3}\left[(V_{\mathrm{u}} - \bar{v}_{\mathrm{T106C}})^3 - (V_{\mathrm{l}} - \bar{v}_{\mathrm{T106C}})^3\right]\mathrm{d}x \tag{3}$$

$$A_{\mathrm{cavity}} = \int_{0.1c}^{0.65c} (C_{\mathrm{u}} - C_{\mathrm{l}})\,\mathrm{d}x \tag{4}$$

$$\bar{v}_{\mathrm{cavity}} = \frac{1}{A_{\mathrm{cavity}}}\left[\int_{0.1c}^{0.65c} \frac{1}{2}(C_{\mathrm{u}}^2 - C_{\mathrm{l}}^2)\,\mathrm{d}x\right] \tag{5}$$

$$I_{\mathrm{cavity}} = \int_{0.1c}^{0.65c} \frac{1}{3}\left[\left(C_{\mathrm{u}} - \bar{v}_{\mathrm{cavity}}\right)^3 - (C_{\mathrm{l}} - \bar{v}_{\mathrm{cavity}})^3\right]\mathrm{d}x \tag{6}$$

$$A_{\mathrm{HB}} = A_{\mathrm{T106C}} - A_{\mathrm{cavity}} \tag{7}$$

$$I_{\mathrm{HB}} = I_{\mathrm{T106C}} - I_{\mathrm{cavity}} \tag{8}$$

The area and moment of inertia can be calculated from Eqs.(1—8) for the hollow blade. They are modeled by using Creo Parametric, CAD software with a 3 mm base plate for numerical and experimental modal analysis (Fig.5).

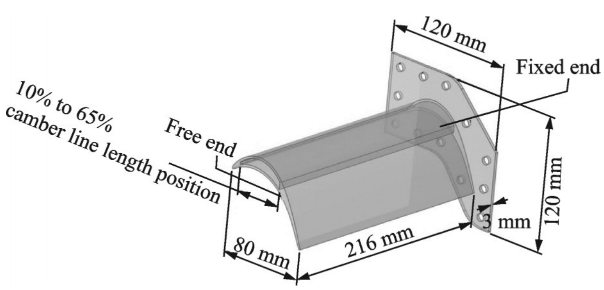

Fig.5 Dimensions of hollow blade geometry with base plate

A BBC lattice structure is introduced into the cavity of the hollow blade. BCC lattice structure is composed of eight struts connected at the center of a cube (Fig.6(a)). According to the study conducted by Feng et al.[38] on BCC lattice structure, they have two advantages. Firstly, the BCC can be well-manufactured because all struts can incline properly. Secondly, it has a simple deform and failure mode under uniaxial and multi-axial compression. Zhao et al.[39] mentioned that the stress distribution of the BCC lattice structure with hexagonal struts was similar to the cylindrical struts. Whereas, the elastic and shear modulus were comparatively high for the hexagonal design (Fig.6(b)), where "a" is the side length, "d" the long diagonal, and "s" the short diagonal of the hexagonal strut. Due to these advantageous properties, BCC with hexagonal struts is used in this study.

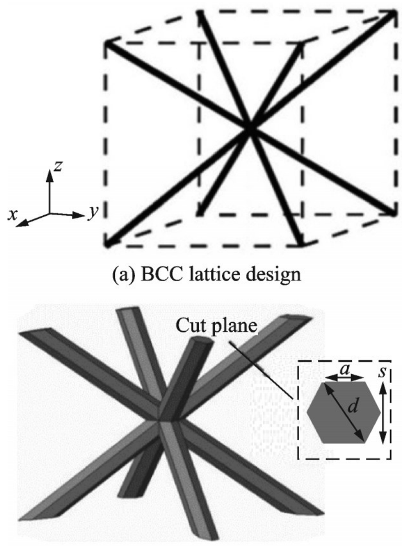

(a) BCC lattice design

(b) BCC with hexagonal struts

Fig.6 BCC lattice structure

Only for this study, the BCC lattice structure is integrated inside the hollow blade at 50% and 80% of the cavity length locations along the whole span. The hexagonal strut short diagonal (s) is kept at 0.8 mm in a 10 mm×10 mm×10 mm unit cell for this study (Fig.7). Due to the camber of the airfoil profile, the struts at 80% location are lesser at the upper surface of the cavity $C_{\mathrm{u}}(x)$ and more at the lower surface of the cavity $C_{\mathrm{l}}(x)$.

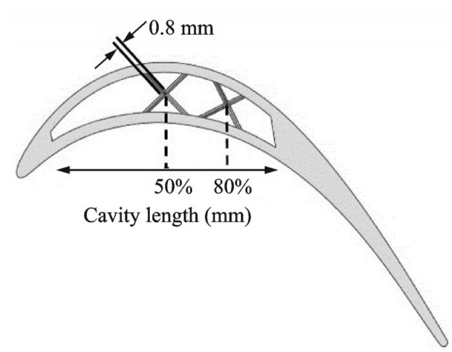

Fig.7 Hexagonal strut BCC lattice structure at 50% and 80% of the cavity length

The BCC lattice will support the cavity and resist deformation, and provide enough stiffness to increase the natural frequencies of the hollow blade. The lattice structure will make the blade a non-prismatic structure, having different cross-sectional areas and area moment of inertia (MOI) through the span. The cross-sectional area and moment of inertia of the BCC can be added to Eq.(7) and Eq.(8) to form the total cross-sectional area Eq.(9) and area moment of inertia Eq.(10) for the BCC blade.

$$A_{\mathrm{BCCB}} = A_{\mathrm{T106C}} - A_{\mathrm{cavity}} + A_{\mathrm{BCC}} \tag{9}$$

$$I_{\mathrm{BCCB}} = I_{\mathrm{T106C}} - I_{\mathrm{cavity}} + I_{\mathrm{BCC}} \tag{10}$$

Fig.8 presents the moment of inertia for a single portion of 10.8 mm for both blades. Due to the incorporation of the BCC structure compared to the hollow blade, the MOI increases for the BCC blade. The MOI for the hollow blade remains the same for the portion and a horizontal line is observed explaining the prismatic behavior of the blade. In the case of the BCC blade, the MOI is higher when the struts are further apart and decreases as they come closer. This trend repeats throughout the entire BCC blade structure. This indicates the non-prismatic behavior of the blade.

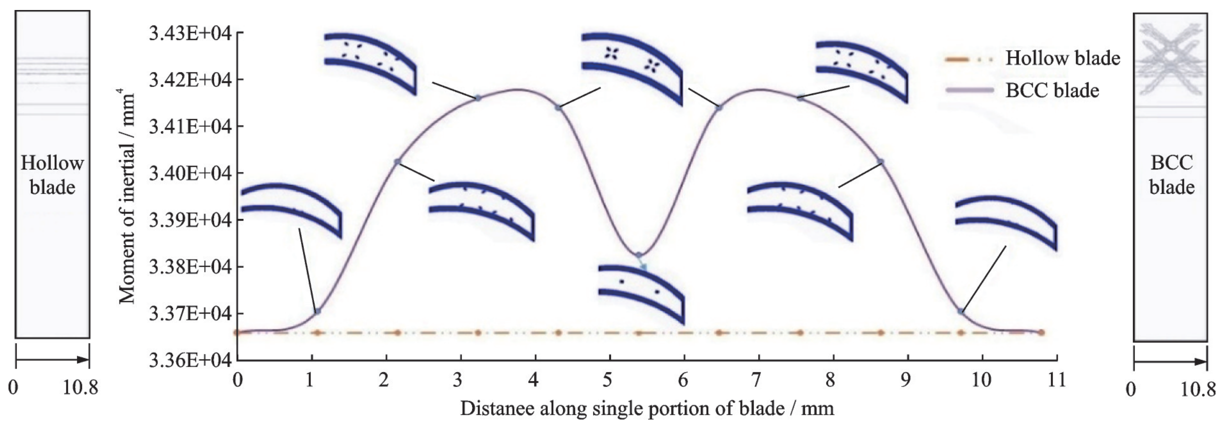

Fig.8 Moment of inertia of hollow and BCC blade of a 10.8 mm portion

The single portion is periodically throughout the blade and enhances the MOI. With the increase in MOI, the stiffness of the blade is enhanced as well which eventually increase the natural frequencies of the hollow blade due to the inclusion of BCC structure. Four blades are additively manufactured: Two from AlSi10Mg and the other from PLA material. The metal blades are manufactured by selective laser melting (SLM) technique, in which laser melts metal powder can form the structures. The PLA blades are manufactured by the fused deposition modeling (FDM) technique, in which the PLA filament is melted down a nozzle and forms different complex structures. The cost of producing metal blades is 90% more than PLA blades in the available market. Fig.9 presents the additive manufactured blades with the BCC lattice structure inside with their mass.

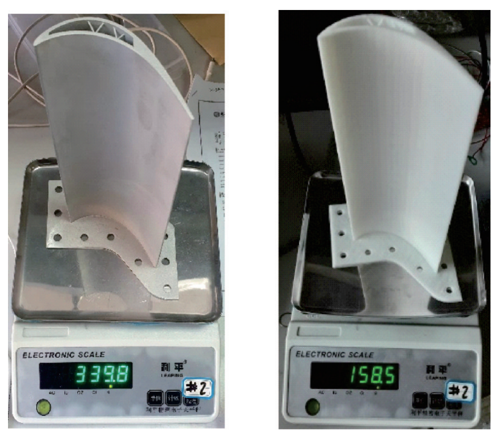

(a) AlSi10Mg BCC blade (b) PLA BCC blade

Fig.9 Mass of the manufactured BCC blades

1.2 Experimental modal testing setup

Modal analysis is conducted to extract the inherent dynamic structural properties (natural frequencies, mode shapes and damping ratio) of a structure and is used to formulate a mathematical model for its dynamic behavior. This mathematical model is considered the modal model and is derived by modal testing. The theoretical basis of this technique entails establishing a connection between the vibration response at one point and the excitation at that or another point on the structure. This relationship is known as frequency response function (FRF) and its combinations from multiple points on the structure lead to a set of FRFs which are represented as the FRF matrix of the system.

The system/structure is divided into multiple points. A sensor is attached to record the maximum response. The input force excites the structure and the response is received in the form of time domain data (acceleration vs. time). Fast Fourier transform (FFT) is used and is converted into FRF (Fig.10). The peaks found in the FRF plot show the excitation frequencies of the structure, having a specific boundary condition. Each peak can be considered as a single degree of freedom (SDOF). Analysis can be performed in the form of a spring-mass-damper system and the analysis can be done for finding the natural frequencies, mode shapes and damping ratios.

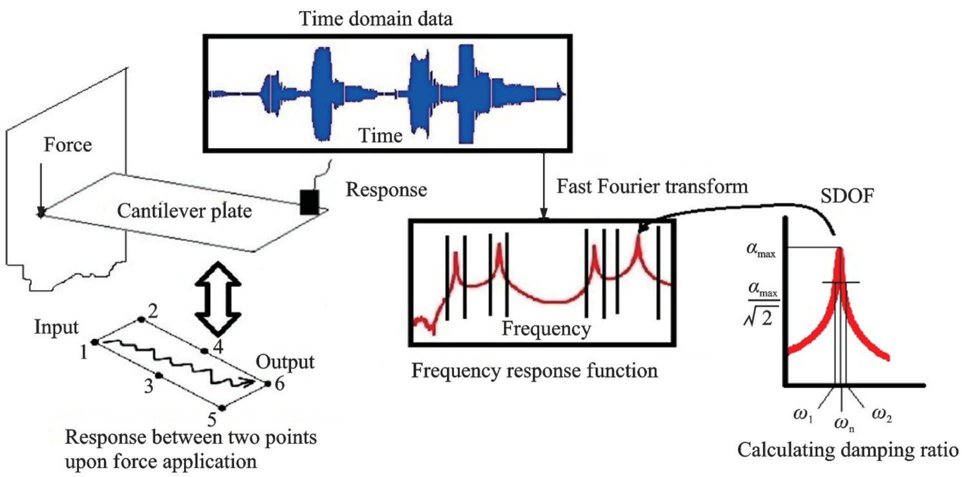

Fig.10 Experimental modal testing and analysis

The damping ratio can be calculated using the half-power bandwidth method which is also known as peak picking method. The maximum amplitude ($\alpha_{\max}$) of the resonating frequency (ω_n) is identified at the peak. Then half-power points ω_1 and ω_2 are located from each side of the peak with amplitude $\left(\alpha_{\max}/\sqrt{2}\right)$ and the damping ratio (ξ) can be calculated as

$$\xi=\frac{\omega_2-\omega_1}{2\omega_n} \tag{11}$$

Four prototype (hollow and BCC) blades of AlSi10Mg and PLA are bolted to the base plate one by one for testing. Twenty-four measurement locations are marked on the convex side (suction side) of the blade. The points (1, 9 and 17) are at a 6 mm distance from the base (fixed side), whereas all other points are approximately spaced at a distance of 30 mm from the fixed to free end and a distance of 40 mm from trailing edge to leading edge (Fig.11). A single reference roving hammer test is performed with a single accelerometer fixed to the free-end tip of the blade trailing edge to measure the response. These points are mapped into the modal software and are excited using a modal hammer (PCB-086C03) with a rubber tip. Each point exhibits a response in the form of acceleration, and the response FRF is observed in the form of accelerance (g/N vs. frequency). The frequency range is set as 0—1 000 Hz. The sampling rate set as 1 024 samples/s and the 1 024 spectral lines are selected. Rectangular window is used which is good for modal hammer impact testing (Fig.12).

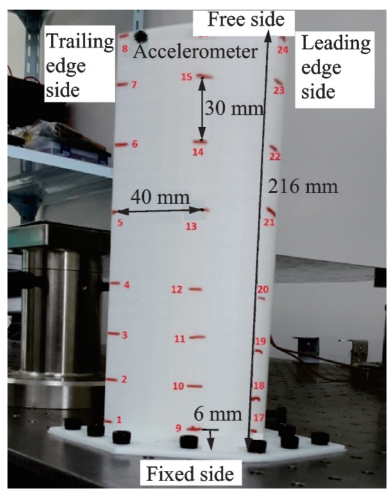

Fig.11 Measurement points of the blade

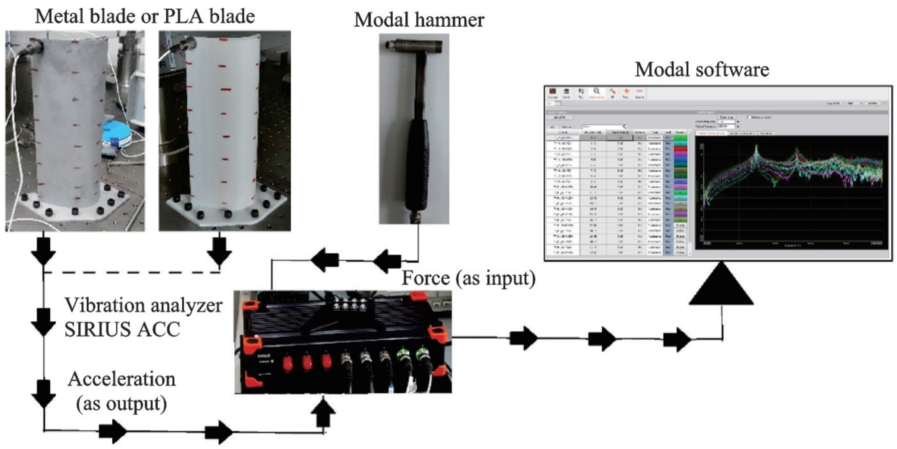

Fig.12 Experimental modal testing flow chart

1.3 Numerical modal analysis setup

Numerical modal analysis (NMA) of the blades is conducted using ANSYS. Modal analysis is performed by using an un-damped free vibration system with the following equation.

$$[\boldsymbol{M}]\{\ddot{x}\}+[\boldsymbol{K}]\{x\}=0 \tag{12}$$

where $[\boldsymbol{M}]$ is the mass matrix, and $[\boldsymbol{K}]$ the stiffness matrix.

For the eigenvalue (natural frequencies), modal analysis is employed

$$\left([\boldsymbol{K}]-\boldsymbol{\omega}_j^2[\boldsymbol{M}]\right)\left\{\boldsymbol{\phi}_j\right\}=0 \tag{13}$$

where $\boldsymbol{\omega}_j^2$ is the angular natural frequencies matrix and $\left\{\boldsymbol{\phi}_j\right\}$ the eigenvectors which are the mode shapes for the corresponding frequencies. The angular frequencies are converted into natural frequencies

$$f=\frac{\boldsymbol{\omega}_j}{2\pi} \tag{14}$$

The models are divided into small elements, which can be represented as a sparse matrix. To solve these sparse matrices, the block lanczo method is employed for extracting the eigenvalues (natural frequencies) and eigenvectors (mode shapes) of the structure[40]. The material properties utilized in this work of AlSi10Mg, PLA, and U-500 are presented in Refs.[8,41-42].

Table 1 Material properties of AlSi10Mg, PLA and U-500 nickel-based alloys

Property	AlSi10Mg	PLA	U-500
Density/(kg·m^{-3})	2 670	1 210—1 250	7 800
Young's modulus/GPa	76.60	0.35—3.50	190—210
Poisson ratio	0.33	0.30	0.27—0.30
Bulk modulus/Pa	$7.607\,8\times10^{10}$	$0.291\,6\times10^{9}$—$1.833\,3\times10^{9}$	1.583×10^{11}
Shear modulus/Pa	$2.917\,3\times10^{10}$	$0.134\,6\times10^{9}$—$0.846\,15\times10^{9}$	7.307×10^{10}

The models are auto-meshed with tetrahedron and mapped-face meshing (over the pressure and suction side) to convert them into quadrilaterals to capture the edges of the blade (Fig.13). The finite element model generated for the hollow blade has 24 053 nodes and 12 279 elements. And there are 166 503 nodes and 87 936 elements for the BCC blade. Fixed boundary condition is applied to the holes in the base plate of models to create the cantilever behavior.

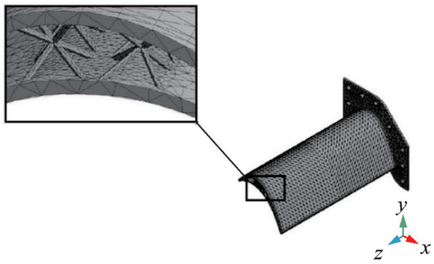

Fig.13 BCC blade meshed model

2 Results and Discussion

2.1 Experimental and numerical modal analysis results of blades

Experimental modal analysis results are obtained in the form of natural frequencies for each blade from the FRF. The FRF plots of aluminum-based hollow (AHB), BCC blade (AXB), PLA-based hollow (PHB) and BCC blade (PXB) are presented in Fig.14 and Fig.15. The EMA response plot of AHB in Fig.14(a) shows two peaks at 280.3 Hz and 503 Hz, which correspond to the first and second natural frequencies of the blade design. The damping ratios at these peaks are 0.28% and 1.5%. Meanwhile, the EMA plot of AXB in Fig.14 (b) shows the peaks at 295.8 Hz and 522.5 Hz, whereas the damping ratios are calculated to be 0.24% and 1.06%.

EMA of the PHB response plot in Fig.15(a)

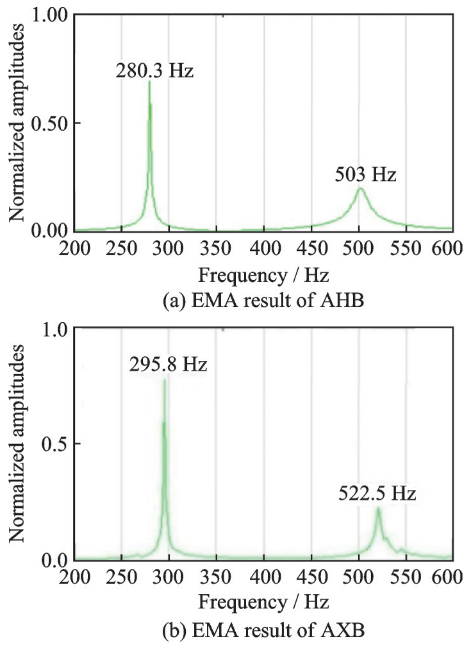

Fig.14 Natural frequencies of aluminum alloy blade

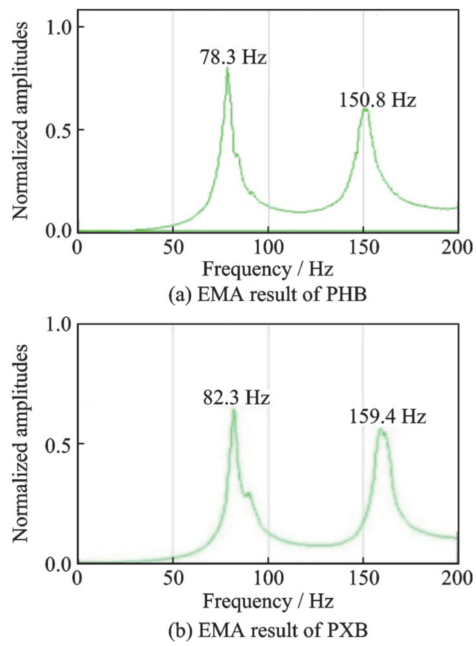

Fig.15 Natural frequencies of PLA blades

shows the first two peaks at 78.3 Hz and 150.8 Hz, which correspond to the first and second natural frequencies. Whereas, the EMA response plot of PXB in Fig.15(b) shows peaks at 82.3 Hz and 159.4 Hz which are the first and second natural frequencies of the PLA BCC lattice blade. The calculated damping ratios for the first and second peaks are 2.64% and 2.63% for the PLA hollow blade, whereas the damping ratios for the PLA BCC blade are calculated to be 2.18% and 2.39%. Table 2 presents the enhanced natural frequencies for the lattice-based turbine blade design, which is a preferable parameter in GTE's.

Table 2 Experimental mass and natural frequencies

Material	Blade type	Mass/g	First-order mode/Hz	Second-order mode/Hz
AlSi10Mg	AHB	332.1	280.3	503.0
	AXB	339.8	295.8	522.5
PLA	PHB	154.5	78.3	150.8
	PXB	158.5	82.3	159.4

The experimental mode shapes of the blade designs of both materials are presented in Fig.16. The first-order mode of the blades is the bending mode in the z-direction, whereas the second-order mode is the torsional mode. It can be observed that the BCC blades have lesser deformation levels than the hollow blade for both bending and torsional mode, presenting that the BCC structure provides stiffness in the cavity and increases the natural frequencies as well as lowers the deformation levels.

The natural frequencies obtained from NMA of the blade designs for three different materials are presented in Table 3. The natural frequencies for the AHB are 277.58 Hz and 499.81 Hz for the first-

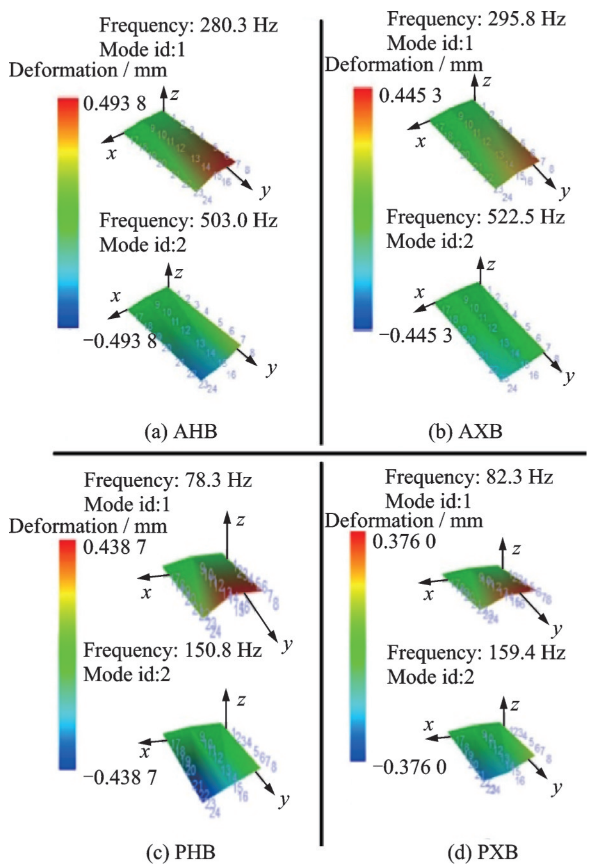

Fig.16 EMA mode shapes of aluminum, PLA material hollow and BCC blades

Table 3 Numerical mass and natural frequencies

Material	Blade type	Mass/g	First-order mode/Hz	Second-order mode/Hz
AlSi10Mg	AHB	329.38	277.58	499.81
	AXB	339.05	294.01	522.23
PLA	PHB	154.20	79.19	153.17
	PXB	158.10	83.89	160.46
U-500	UHB	962.23	294.61	569.84
	UXB	990.48	311.36	596.78

order and second-order modes respectively. While the natural frequencies are also increased for the AXB blade, where the first-order mode is 294.01 Hz and the second-order mode is 522.23 Hz. Similarly, the natural frequencies enhance for the PLA blade. The first-order mode of the hollow blade (PHB) is 79.19 Hz and the second-order mode is 153.17 Hz, whereas the first-order mode for the PXB is 83.893 Hz and 160.46 Hz for the second-order mode. The natural frequencies for the U-500 material for the hollow blade (UHB) are 294.61 Hz and 569.84 Hz, whereas the inherent frequencies for the U-500 BCC blade (UXB) are 311.36 Hz and 596.78 Hz for the first and second-order modes.

The first-order mode is the bending mode, whereas the second-order mode is the torsional mode. Max deformation at the trailing edge is observed for the first-order mode. Whereas, the blade twists from the nodal line at the middle for second-order mode (Fig.17).

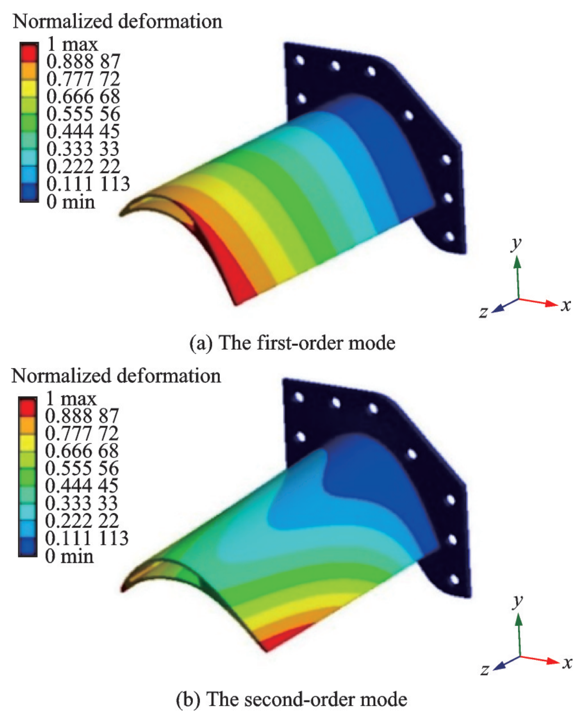

Fig.17 Mode shapes for the hollow blade

Fig.18 presents the numerical modal shapes of the BCC blades. Lesser volume has deformation in the first-order mode of the BCC blade as compared to the hollow blade. This is due to the BCC increases the stiffness of the blade. The deformation for the second-order mode (torsional mode) is nearly the same. When comparing both responses, it can be seen that the inclusion of the BCC lattice structure inside the blade enhances the natural frequencies of the blade. EMA indicates that the usage of a lattice structure is beneficial for the turbine blade. It increases the natural frequencies. And it is always desirable to have higher blade natural frequencies to avoid resonance with the rotational speeds of the GTE[23].

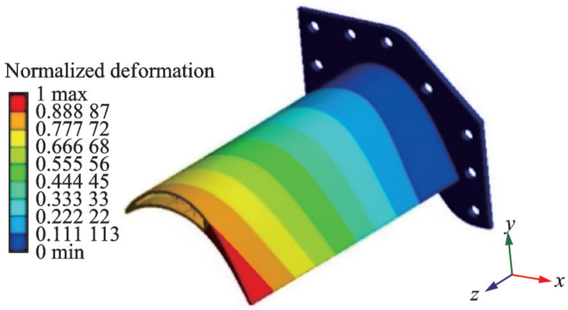

(a) The first-order mode

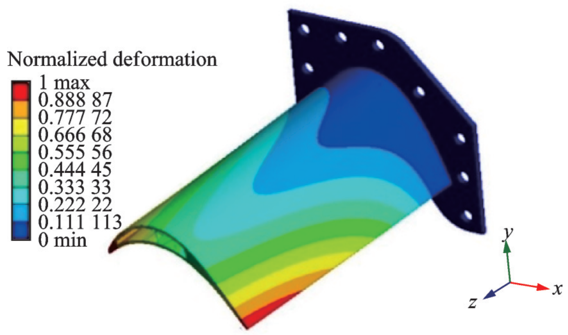

(b) The second-order mode

Fig.18 Mode shapes for the BCC blade

2.2 Comparison of percent change results for different methods

Table 4 presents the percent change values for modified blades that are made from different materials. These values demonstrate the percentage difference between the old and new values. For the aluminum alloy material, the experimental difference is 2.32% in terms of mass, and 2.93% in numerical terms. Similarly, for the PLA material, the percent change for experimental blades is 2.58% and 2.53%. In first-order mode, the experimental difference for aluminum alloy material is 5.53%, while the numerical difference is 5.95%. For PLA material, the experimental percent change is 5.11%, and the numerical result is 5.93%. As for the second-order mode, the percent change ranges from 4% to 5.7%. Lastly, the numerical percent change for U-500 blades show that the mass change is 2.93%, whereas, for the first and second-order modes, they are 5.68% and 4.73%, respectively.

Table 4 Comparison of percent change results between different methods

Modal analysis method	Percent change between mass of both blades/%	Percent change between the first-order mode of both blades/%	Percent change between the second-order mode of both blades/%
Experimental result for AlSi10Mg blades	2.32	5.53	4.01
Numerical result for AlSi10Mg blades	2.93	5.95	4.48
Experimental result for PLA blades	2.58	5.11	5.70
Numerical result for PLA blades	2.53	5.93	4.75
Numerical result for U-500 blades	2.93	5.68	4.73

The turbine blade made out of aluminum alloy and the one made out of PLA exhibit similar behavior, regardless of the material used. The findings show that even when a different material (U-500) is used, the percentage change is almost the same as the PLA and aluminum material. These observations confirm that no matter the material used, the similitude behavior of the similar structure of the turbine blade remains almost identical.

By keeping the structural geometry and boundary conditions identical, it is possible to achieve a nearly identical percent change between two designs, irrespective of the material used. Even if the material is changed, the percent change between the designs remains unaffected. The PLA material provides a cost-effective solution for designing and fabricating turbine blades for research purposes. It can be seen that the aluminum BCC blade enhances the natural frequencies compared to the aluminum hollow blade, and also demonstrates that using PLA material can produce results that are comparable to expensive metal blades. With this technique, prototypes can be designed, fabricated and performed EMA, which can help to create more efficient and cost-effective solutions for enhancing natural frequencies.

3 Conclusions

Metal additive manufacturing has introduced a new way of building complex lattice-based aerospace-grade parts in a significantly reduced timeframe. However, metal prints and experiments required for design evaluation are still costly.

In the current project, an economical method of designing evaluation for expensive turbine blades has been proposed in the current project. This is achieved by evaluating and comparing the vibrational characteristics trends of the PLA and metal-manufactured blades. For this purpose, a T106C LPT blade is structurally modified by internally integrated BCC lattices to reduce the weight and improve the vibrational characteristics.

EMA and NMA are conducted on two designs (hollow, BCC blade) of different materials. The results are compared based on the percent change of natural frequencies. Subsequently, a nickel alloy (U-500) model is numerically analyzed, compared with the results of aluminum and PLA materials. Based on the findings, the following conclusions can be drawn:

(1) By incorporating a lattice structure within the hollow blade, the natural frequencies improve by 5.9% for the first-order mode and 4.7% for the second-order mode with only 2.5% mass inclusion.

(2) A maximum percent change of 1.9% is observed between the EMA and NMA results, giving a good agreement of the obtained results.

(3) The comparison between the numerical and experimental results reveals similar trends in terms of the percentage change in mass and natural frequencies.

(4) The NMA of the nickel-based alloy U-500 blade shows the same behavior in percent change for the first and second natural frequencies, which is similar to the PLA and aluminum prototypes.

The similitude behavior between the PLA models and metal models is quite effective in predicting the comparative design values for selection and additive manufacturing. According to the available technology in the market, metal printing is 90% more expensive compared to PLA printing which is the novelty of this research.

In conclusion, both numerical and experimental modal analyses indicate that the percent change trend of mass and natural frequencies between the metallic turbine blades can be verified by the PLA-printed prototypes, indicating a similar trend. These results contribute to the development of a novel validation method for complex designs, utilizing a similarity behavior model. According to this model, when a structure is subjected to the same boundary conditions, it will exhibit the same percentage change in vibrational characteristics, regardless of the material used. This method provides a valuable approach for validating complex designs based on their similarity in vibrational behavior.

References

[1] DAR U A, MIAN H H, ABID M, et al. Experimental and numerical investigation of compressive behavior of lattice structures manufactured through projection micro stereolithography[J]. Materials Today Communications, 2020, 25: 101563.

[2] RIVA L, GINESTRA P S, CERETTI E. Mechanical characterization and properties of laser-based powder bed-fused lattice structures: A review[J]. The International Journal of Advanced Manufacturing Technology, 2021, 113: 649-671.

[3] KULANGARA A J, RAO C S P, BOSE P S C. Generation and optimization of lattice structure on a spur gear[J]. Materials Today: Proceedings, 2018, 5: 5068-5073.

[4] YIN S, CHEN H, WU Y, et al. Introducing composite lattice core sandwich structure as an alternative proposal for engine hood[J]. Composite Structures, 2018,201: 131-140.

[5] MAGERRAMOVA L, VOLKO M G, AFONIN A, et al. Application of light lattice structures for gas turbine engine fan blades[C]// Proceedings of the 31st Congress of International Council of the Aeronautical Sciences (ICAS). Belo Horizonte:[s.n.], 2018.

[6] DU Y X, GU D, XI L, et al. Laser additive manufacturing of bio-inspired lattice structure: Forming quality, microstructure and energy absorption behavior[J]. Materials Science and Engineering A—Structural Materials Properties Microstructure and Processing, 2020, 773:138857.

[7] STIEGER R D. The effects of wakes on separating boundary layers in low-pressure turbines[D]. Cam-

bridge: Cambridge University Peterhouse, 2002.

[8] EFE-ONONEME O E, IKPE A E, ARIAVIE G O. Modal analysis of conventional gas turbine blade materials (udimet 500 and in738) for industrial applications[J]. Journal of Engineering Technology and Applied Sciences, 2018, 3(2): 119-133.

[9] KHAN S A, ARIF I, SAFDAR M U. Determination and comparison of modal parameters of a high lifting low-pressure turbine blade under Ni-based superalloys using computational modal analysis[C]//Proceedings of International Bhurban Conference on Applied Sciences and Technologies (IBCAST). Islamabad: IEEE, 2021: 169-176.

[10] BENINI E. Advances in gas turbine technology[M]. [S.1.]: InTech, 2011:293-314.

[11] DONOVAN M H, RUMPFKEIL M P, MARKS C R, et al. Investigation of elevated turbulence on high-lift low pressure turbine endwall flows[C]// Proceedings of AIAA Scitech 2021 Forum. [S. 1.] : AIAA, 2021.

[12] HOWELL R J, RAMESH O N, HODSON H P, et al. High lift and aft-loaded profiles for low-pressure turbines[J]. Journal of Turbomachinery, 2000, 123(2): 181-188.

[13] NAUNG S W, NAKHCHI M E, RAHMATI M. Prediction of flutter effects on transient flow structure and aeroelasticity of low-pressure turbine cascade using direct numerical simulations[J]. Aerospace Science and Technology, 2021, 119: 107151.

[14] ANTORKAS S, MASSINI M, MONTOMOLI F. Topology optimization of gas turbine blades[C]//Proceedings of Global Power and Propulsion Society. Chania:[s.n.], 2021.

[15] BHAGI L K, GUPTA P, RASTOGI V. A brief review on failure of turbine blades[C]//Proceedings of Smart Technologies for Mechanical Engineering. Delhi:[s.n.], 2013.

[16] EWINS D. Modal testing: Theory and practice[M]. New York: Wiley, 1995.

[17] HE J, FU Z. Modal analysis[M]. Oxford: Butterworth-Heinemann, 2001: 1-11.

[18] CASABURO A, PETRONE G, FRANCO F, et al. A review of similitude methods for structural engineering[J]. Applied Mechanics Reviews, 2019, 71(3): 030802.

[19] PRIYA T, KUMAR S, PRATAP D, et al. Rotor blade vibration measurement on aero gas turbine engines[C]//Proceedings of the National Aerospace Propulsion Conference. Singapore: Springer, 2022: 263-273.

[20] LEE D, BAE Y, KIM H, et al. Vibration analysis of a low-pressure turbine bladed disk in 500 MW fossil power plants[C]//Proceedings of Meetings on Acoustics. Portland,Oregon: AIP(ASA), 2009.

[21] NIRMALKUMAR G, KUMAR C V S, VENKATESH S. Experimental modal analysis of compressor rotor blades[C]//Proceedings of the 3rd International Conference on Frontiers in Automobile and Mechanical Engineering (FAME). Chennai:AIP, 2020.

[22] OSIEWICZ M, CIEŚLAK S, BIELECKI M. Determination of the geometric properties of a jet engine fan blades based on modal vibration testing[J]. Transactions on Aerospace Research, 2022, 268(3): 56-74.

[23] PRESAS A, VALENTÍN D, VALERO C, et al. Experimental measurements of the natural frequencies and mode shapes of rotating disk-blades-disk assemblies from the stationary frame[J]. Applied Sciences, 2019, 9(18): 3864.

[24] PRZYSOWA R. Blade vibration monitoring in a low-pressure steam turbine[C]//Proceedings of ASME Turbo Expo: Turbomachinery Technical Conference and Exposition. Oslo,Norway: ASME, 2018.

[25] RANI S, AGRAWAL A, RASTOGI V. Vibration analysis for detecting failure mode and crack location in first stage gas turbine blade[J]. Journal of Mechanical Science and Technology, 2018, 33: 1-10.

[26] SHETKAR K A D R, SRINIVAS J. Analytical modeling and vibration analysis of the last-stage LP steam turbine blade made of functionally graded material[J]. Arabian Journal for Science and Engineering, 2021, 46: 7363-7377.

[27] SHUKLA A K, HARSHA S P. Vibration response analysis of last stage LP turbine blades for variable size of crack in root[J]. Procedia Technology, 2016, 23: 232-239.

[28] VERHEES M L J. Experimental modal analysis of a turbine blade[R]. [S.l.]: [s.n.], 2004.

[29] WITOŚ M. On the modal analysis of a cracking compressor blade[J]. Research Works of Air Force Institue of Technology (AFIT), 2008,23(1): 21-36.

[30] WITOŚ M, STEFANIUK M. Compressor blade fatigue diagnotics and modelling with the use of modal analysis[J]. Fatigue of Aircraft Structures, 2011, 1(3): 112-133.

[31] WITO M. High sensitive methods for health monitoring of compressor blades and fatigue detection[J]. The Scientific World Journal, 2013, 29: 218460.

[32] YANG Y, XIANG H, GAO J, et al. Experimental study of the vibration phenomenon of compressor rotor blade induced by inlet probe support[J]. Journal of Thermal Science, 2021, 30(5): 1674-1683.

[33] HUSSAIN S, GHOPA W A W, SINGH S S K, et al. Experimental and numerical vibration analysis of octet-truss-lattice-based gas turbine blades[J]. Metals, 2022, 12(2): 340.

[34] HUSSAIN S, GHOPA W A W, SINGH S S K, et al. Vibration-based fatigue analysis of octet-truss lattice infill blades for utilization in turbine rotors[J]. Materials, 2022, 15(14): 4888.

[35] BIAN Y, YANG F, ZHANG S, et al. Similarities of the mechanical responses of body-centered cubic lattice structures with different constituent materials under compression[J]. JOM, 2022, 74(4): 1774-1783.

[36] MOURIAUX S, PURI K. High-lift low pressure turbines T106-A and T106-C[J]. Notes on Numerical Fluid Mechanics and Multidisciplinary Design, 2021, 148: 465-477.

[37] DEMIRTAS A, BAYRAKTAR M. Free vibration analysis of an aircraft wing by conisdering as a cantilever beam[J]. Selcuk University Journal of Engineering Science Technology, 2019, 7(1): 12-21.

[38] FENG Q, TANG Q, LIU Z, et al. An investigation of the mechanical properties of metallic lattice structures fabricated using selective laser melting[J]. Proceedings of the Institution of Mechanical Engineers, Part B: Journal of Engineering Manufacture, 2018, 232(10): 1719-1730.

[39] ZHAO M, ZHANG D Z, LI Z, et al. Design, mechanical properties, and optimization of BCC lattice structures with taper struts[J]. Composite Structures, 2022, 295: 115830.

[40] BHAMU R K, SHUKLA A, SHARMA S C, et al. Low-cycle fatigue life prediction of LP steam turbine blade for various blade-rotor fixity conditions[J]. Journal of Failure Analysis and Prevention, 2021, 21: 2256-2277.

[41] AIDRO. Material data sheet: AlSi10Mg[EB/OL]. (2022-01-25). https://aidro.it/wp-content/uploads/2022/01/AlSi10Mg-1.pdf.

[42] FARAH S, ANDERSON D G, LANGER R S. Physical and mechanical properties of PLA, and their functions in widespread applications—A comprehensive review[J]. Advanced Drug Delivery Reviews, 2016, 107: 367-392.

Acknowledgement This work was supported by the National Natural Science Foundation of China (No. 12111540251).

Authors Mr. **MUHAMMAD Usman Safdar** received the B.S. degree in mechanical engineering in 2012 from HITEC University, Taxila, Pakistan, and the M.S. degree in Aerospace Engineering from Air University, Islamabad, Pakistan, in 2015, respectively. He has been pursuing the Ph.D. degree in aerospace engineering since 2021 in State Key Lab of Mechanics and Control for Aerospace Structures, College of Aeronautics, Nanjing University of Aeronautics and Astronautics. He is mainly engaged in the topic of fluid-structure interaction of lattice-based turbine blades for gas turbine engines.

Prof. **SHEN Xing** received the Ph.D. degree in aerospace engineering from Nanjing University of Aeronautics and Astronautics and did Post-Doctorate from Korea Advanced Institute of Science and Technology (KAIST) in 2007—2008, respectively. He is mainly engaged in the design, preparation, testing and application research of new sensors and drives based on piezoelectric and shape memory alloys and their application in aeronautical intelligent structures. Currently, he is a visiting research scholar at Graduate School of Chinese Aeronautical Establishment.

Authors contributions Mr. **MUHAMMAD Usman Safdar** conceptualized, modeled, conducted numerical and experimental testing, interpreted the results, and wrote the manuscript. Prof. **SHEN Xing** supervised the concept and testing techniques, proof-reading and funded the project. Dr. **EIMAN B. Saheby** co-supervised the concept and testing techniques with proof-reading the manuscript. All authors commented on the manuscript draft and approved the submission.

Competing interests The authors declare no competing interests.

(Production Editors: XU Chengting, WANG Jie)

增材制造涡轮叶片自然频率相似行为的评估

MUHAMMAD Usman Safdar[1]，沈 星[2]，EIMAN B. Saheby[1]

（1.南京航空航天大学航空学院,航空航天结构力学与控制国家重点实验室,南京 210016,中国；
2.中国航空研究院研究生院,扬州 225111,中国）

摘要：结构性能的改进涉及对新旧设计模型所选参数的比较,计算它们之间的百分比变化是一种评估方法。本文提出了一种具有成本效益的方法,生成基于增材制造铝合金(AlSi10Mg)的体心立方晶格(Body-centered cubic lattice, BCC)涡轮叶片(T106C)与聚乳酸(Poly-lactic acid, PLA)材料中的相同物质,比较固有频率下的百分比变化。首先,在涡轮叶片(空心叶片)内部形成一个空腔。然后,将腔体长度的50%和80%的BCC掺入两种材料的空心叶片中,获得固有频率。金属叶片的制造成本比PLA叶片高出90%,而两种材料叶片设计显示出相似的百分比变化,一阶模式的增强超过了5%,二阶模式的增强超过了4%。为了观察另一种材料,使用镍基U-500材料对两个叶片进行了数值分析,取得了相同的结果。结果说明可以使用PLA材料验证设计之间的百分比变化。

关键词：AlSi10Mg;聚乳酸;U-500;T106C刀片;BCC晶格结构